Hindawi
International Journal of Chemical Engineering
Volume 2022, Article ID 5072635, 18 pages
https://doi.org/10.1155/2022/5072635

Research Article

Characterization and Optimization of Calcination Process Parameters for Extraction of Aluminum from Ethiopian Kaolinite

Adamu Esubalew Kassa,[1] **Nurelegne Tefera Shibeshi**,[2] **and Belachew Zegale Tizazu**[1]

[1]*Department of Chemical Engineering, Addis Ababa Science and Technology University, P. O. Box 16417, Addis Ababa, Ethiopia*
[2]*School of Chemical and Bio-engineering, Addis Ababa Institute of Technology, Addis Ababa University, Addis Ababa, Ethiopia*

Correspondence should be addressed to Nurelegne Tefera Shibeshi; nurelegne.tefera@aait.edu.et

Received 14 December 2021; Revised 22 January 2022; Accepted 16 February 2022; Published 10 March 2022

Academic Editor: Eric Guibal

The present study aimed to optimize the calcination process parameters (viz., temperature, time, and particles size) for the extraction of aluminum from Ethiopian kaolinite. The kaolinite calcination was done in the temperature of 600–700°C, time of 120–180 min, and particles size of 106–355 μm. The extraction of aluminum from calcined kaolinite was carried out at fixed acid concentration of 3 M, temperature of 80°C, liquid-to-solid ratio of 12 mL g^{-1}, time of 120 min, and stirring speed of 700 rpm. The chemical composition of kaolinite was determined using XRF. Moreover, kaolinite, metakaolinite, and extracted aluminum were characterized by XRD, TGA, DSC, and FTIR. The XRF result of the kaolinite was mainly silicon oxide (55.76% w/w), aluminum oxide (32.02% w/w), and loss on ignition (11.17% w/w). Calcination of kaolinite produced amorphous metakaolinite due to the dehydroxylation reaction as shown by the FTIR results. Three endothermic peaks and one exothermic peak were detected in the thermal analysis of the kaolinite due to water removal, impurities decomposition, dehydroxylation reaction, and phase change from metakaolinite to spinel, respectively. The extracted aluminum proportionally increased with kaolinite calcination temperature and time. However, the extracted aluminum increased as the particles size reduced. The extracted aluminum was in the form of aluminum chloride hexahydrate and trigonal crystalline structure. The optimum values of the degree of conversion of kaolinite dehydroxylation reaction and extracted aluminum of 0.992 and 71.28% w/w were obtained at the optimum kaolinite calcination temperature of 700°C, time of 180 min, and particles size of 106 μm, respectively.

1. Introduction

The global increase of aluminum demand resulted in attention of developing alternative extraction methods to produce aluminum from nonbauxite ores [1]. Moreover, due to the limited availability of bauxite in most countries and high content of iron in the bauxite, researchers have been looking for possible alternative raw materials for aluminum extraction, such as kaolinite [2]. Kaolinite mineral is mainly made up of tetrahedral (SiO_4) and octahedral (AlO_6) sheets, which form elemental clusters constructed on the tetrahedral-octahedral combination [3]. The mineral structure is built up among the elemental clusters through the hydrogen bond provided by hydroxyl ions (OH^-) of the octahedral sheets [4]. The crystalline kaolinite structure (Al_2O_3 $2SiO_2$ $2H_2O$) has been changed to amorphous metakaolinite (Al_2O_3 $2SiO_2$) phase during calcination [5]. The kaolinite dehydroxylation reaction involves the removal of chemically bonded water to produce metakaolinite as shown in equation (1), and the formation of metakaolinite during kaolinite calcination was determined in terms of degree of conversion [6]. The degree of conversion of kaolinite dehydroxylation reaction could be determined from the mass loss of the kaolinite during calcination and the mass loss (loss on ignition) from thermogravimetry analysis (equation (2)) [7].

$$Al_2Si_2O_5(OH)_4(s) \longrightarrow Al_2Si_2O_7(s) + 2H_2O(g)\uparrow \quad (1)$$

$$Y = 1 - \frac{m_s}{m_{s\,\max}}, \quad (2)$$

where Y is the kaolinite dehydroxylation reaction degree of conversion, m_s is the residual mass loss of a sample (g), and m_{smax} is the maximum mass loss (g), which is equal to loss on ignition.

The metakaolinite is more active and easier to react with acid than the kaolinite for extraction of aluminum [8]. The calcination kaolinite activated the aluminum oxide layer within the kaolinite structure which could accelerate the extraction of aluminum with acid dissolution [9]. The extraction yield of aluminum enhanced through the formation of metakaolinite via calcination [10]. The extraction of aluminum from metakaolinite could be carried out using mineral acids such as hydrochloric acid, sulfuric acid, and nitric acid [11–13]. The rate of extraction of aluminum from metakaolinite has been fastest with hydrochloric acid and slowest with nitric acid. Moreover, the hydrochloric acid extraction method has been suitable for selective separation of aluminum chloride from slurry solutions during the filtration process [2, 14, 15]. The main reaction of metakaolinite with hydrochloric acid is given by the following equation [16].

$$Al_2O_3 2SiO_2\,(s) + 6HCl\,(l) \longrightarrow 2AlCl_3\,(l) + 3H_2O\,(l) + 2SiO_2\,(s)\downarrow \quad (3)$$

The degree of conversion of kaolinite dehydroxylation reaction and extraction of aluminum from calcined kaolinite have been affected by various parameters such as calcination temperature, time, and particles size [17–21]. The extraction yield of aluminum has been proportionately increased with calcination temperature and time [1]. The extraction of aluminum and degree of conversion of dehydroxylation reaction increased as the kaolinite calcination temperature was raised from 400 to 900°C, and the extraction of aluminum decreased sharply as the calcination temperature increased over 900°C, although the degree of conversion increased slightly [22, 23]. The extraction yield of aluminum has increased as the particles size reduced which could have a larger surface area to be exposed for acid attack [24]. The extraction yield of aluminum varied from 63 to 91.3% as the calcination temperature, time, and particle sizes of kaolinite from various origins varies from 600 to 850°C, 60–240 min, and 45–210 μm, respectively [17,25–27].

Several studies have been carried out on Ethiopian kaolinite for various applications such as synthesis of zeolite [28, 29]; adsorbent preparation [30], and ceramic membrane synthesis [31]. However, in the authors' knowledge, the effects of calcination temperature, time, and particles size on the degree of conversion of dehydroxylation reaction of kaolinite and extraction yield of aluminum from Ethiopian kaolinite have not been investigated. Hence, the present work aimed to optimize the kaolinite calcination parameters, viz., calcination temperature, time, and particles size of Ethiopian kaolinite on both the degree of conversion of kaolinite dehydroxylation reaction and extraction yield of aluminum using hydrochloric acid. The chemical composition of kaolinite was determined using X-ray fluorescence (XRF). Furthermore, the kaolinite, metakaolinite, and extracted aluminum were characterized by the X-ray diffractometer (XRD), Fourier transformer infrared spectrometer (FTIR), differential scanning calorimeter (DSC), thermogravimetry analyzer (TGA), and ultraviolet-visible spectrophotometer (UV-vis).

2. Materials and Methods

2.1. Kaolinite Pretreatment and Calcination. The raw kaolinite was collected from Awash Melkassa Aluminum Sulphate and Sulfuric Acid Share Company, Ethiopia. The quarry site of kaolinite is Shakiso, which is located 5° 45′N, 38° 55′E, Southern Ethiopia. The kaolinite pretreatment was conducted using procedures of Mirwan et al. [13] with some modifications. The raw kaolinite was soaked in ultrapure water to remove impurities and debris. The kaolinite was dispersed in water, and the insoluble solid residue was discarded. The dispersion was left overnight to separate the wet kaolinite and supernatant liquid. The wet kaolinite was dried with sunlight for 24 h and in the oven for 24 h at 105°C. The dried kaolinite samples were milled and sieved to the required particles size using sieve analyzer (Elettronica Veneta S.P.A, Italy).

The calcination of kaolinite was carried out using the muffle furnace (MF 106, Turkey). The kaolinite samples were calcined at the specified calcination conditions using ceramics crucibles. The calcination process parameters, viz., temperature (600–700°C), time (120–180 min), and particles size (106–355 μm) were taken to optimize calcination condition on the degree of conversion of kaolinite dehydroxylation reaction and extraction yield of aluminum. Moreover, the extraction of aluminum from the calcined kaolinite samples was conducted at fixed extraction conditions, viz., acid concentration = 3 M, liquid-to-solid ratio = 12 mL g^{-1}, temperature = 80°C, time = 120 min, and stirring speed = 700 rpm. Table 1 provides the central composite design (CCD) of kaolinite calcination parameters in the form of coded and actual values. The responses were the degree of conversion of kaolinite dehydroxylation reaction, Y, and extracted aluminum, Z (% w/w).

2.2. Aluminum Extraction, Separation, and Crystallization. The extraction of aluminum was conducted with hydrochloric acid [2, 32, 33]. The hydrochloric acid (37%) was used to prepare hydrochloric acid solutions. The extraction of aluminum was carried out using the digital hotplate magnetic stirrer (DLAB, MS-H280-Pro, China) with a 250 mL glass flask which was connected with a reflux condenser. In each experimental run, 150 mL of 3 M hydrochloric acid solution and 12.5 g of metakaolinite samples were used. The extraction of aluminum was carried out at fixed extraction process parameters, viz., acid concentration = 3 M, liquid to solid ratio = 12 mL g^{-1}, temperature = 80°C, time = 120 min, and stirring speed = 700 rpm. The extracted aluminum solution was separated from the slurry using centrifuge (PrO-Analytical C2004, United Kingdom) at 2000 rpm for 15 min. The filtrate was evaporated and crystallized using the vacuum rotary evaporator (ML-E14-2050, India) at 70°C and 50 rpm. Crystals of

Table 1: Experimental level for central composite design (CCD) in coded and actual values.

Factors	Coded factors	Coded values		Actual values	
		Low	High	Low	High
Temperature (°C)	X_1	−1	+1	600	700
Time (min)	X_2	−1	+1	120	180
Particles size (μm)	X_3	−1	+1	106	355

aluminum were formed in the concentrated solution. The crystals of aluminum were separated from concentrated solution and kept on plastic sheets for 48 h. The partially dried crystals of aluminum were finally dried in the oven (TD-1315, United Kingdom) at 70°C for 3 h. The dried samples were stored in tightly closed plastic bags for further analysis.

2.3. Characterization of Kaolinite, Metakaolinite, and Extracted Aluminum. The chemical composition of kaolinite was determined using X-ray fluorescence (XRF). The crystalline structure, functional groups, and thermal properties of kaolinite, metakaolinite, and extracted aluminum were characterized by X-ray diffraction (XRD), Fourier transformer infrared spectrometer (FTIR), differential scanning calorimetry (DSC), and thermogravimetry analyzer (TGA), respectively [34, 35]. In addition, the concentration of extracted aluminum in the solution was also determined using the ultraviolet-visible spectrophotometer (UV-vis) [36]. The standard aluminum chloride hexahydrate (Blulux analytical reagent aluminum chloride hexahydrate, 99%) was used for comparison.

2.3.1. Characterization Using X-Ray Fluorescence. The chemical composition of kaolinite determined using X-ray fluorescence (XRF, Olympus BTX-528, USA) at cooling temperature of −45°C, 1.54 nm wavelength of kαCu anode, and X-ray tube voltage of 30 kV.

2.3.2. Characterization Using X-Ray Diffraction. The crystalline structures of kaolinite, metakaolinite, and extracted aluminum samples were characterized by X-ray diffraction (Shimadzu XRD-7000, Japan) at cooling temperature of −45°C, 1.54 nm wavelength of kαCu anode, X-ray tube voltage of 40 kV, and the specimens were step-scanned at the rate of 3°min^{-1} with 2θ angles from 5 to 70°.

2.3.3. Characterization Using the Fourier Transformer Infrared Spectrometer. The functional groups present in the kaolinite, metakaolinite, and extracted aluminum samples were characterized by the Fourier transformer infrared spectrometer with attenuation total reflection (FTIR-ATR) detector of DTGS KBr (Thermo Scientific, iS50 ABX smart iTX). The samples were scanned at wavenumber absorption bands from 4000 to 400 cm^{-1}, 32 numbers of scans, and 16 cm^{-1} resolution. The metakaolinite samples which were formed at 600, 650, and 700°C and kaolinite samples were used for FTIR analysis. The functional groups were compared with the characteristics bands which have been reported [4, 37]. Moreover, the functional groups present in the extracted aluminum and standard aluminum chloride hexahydrate samples were determined and compared with the wavenumber absorption bands of known functional groups in previously published reports [38, 39].

2.3.4. Characterization Using Differential Scanning Calorimetry. The thermal properties of kaolinite and extracted aluminum samples were characterized using the differential scanning calorimeter (SKZ1052B, China). The heating rate was 10°C min^{-1} from 25 to 600°C under nitrogen gas atmosphere at the flow rate of 120 mL min^{-1} for differential scanning calorimeter (DSC) analysis. 20 mg of each sample was loaded into the furnace, a ceramics crucible, and an empty ceramic crucible was used as the reference. The enthalpies of endothermic peaks were determined from the DSC peak area.

2.3.5. Characterization Using the Thermogravimetry Analyzer. The mass loss and thermal characteristics of kaolinite, extracted aluminum, and standard aluminum chloride hexahydrate samples were characterized by the thermogravimetry analyzer (SHIMDZU DTG-60H, Japan). The samples were scanned from 25 to 1100°C at 15°C min^{-1} under nitrogen gas atmosphere with flow rate of 50 mL min^{-1} for thermogravimetry analysis (TGA) and differential thermogravimetry analysis (DTA). The mass of kaolinite and extracted aluminum samples for TGA analysis was 13.5 mg and 15 mg, respectively. The endothermic peaks due to thermal decomposition of the samples were identified. Moreover, the degree of conversion of kaolinite dehydroxylation reaction was determined from the mass loss of samples during calcination and the loss on ignition from TGA analysis using equation (2) [7].

2.3.6. Determination of Aluminum Concentration Using the Ultraviolet-Visible Spectrophotometer. The extracted aluminum content in the solution was determined by the ultraviolet-visible spectrophotometer (UV-vis). The absorbance of extracted aluminum and standard solutions were measured using the UV-visible spectrometer (JASCO V-770, Japan). The aluminum concentration of 60 mg L^{-1} was prepared from Blulux analytical reagent aluminum chloride hexahydrate (99%) using ultrapure water as the standard stock solution (1000 mL). The stock solution was diluted to 10 mg L^{-1} of aluminum. The reagent eriochrome cyanine red (ECR) dye ($C_{23}H_{15}Na_3O_9S$) of 0.2 mM was prepared with stock solution of 500 mL. Furthermore, sodium acetate buffer solution of 0.1 M was also prepared from sodium acetate trihydrate ($CH_3COONa\ 3H_2O$) with stock solution of 1000 mL. Then after, 30 mL standard solution of 10 mg L^{-1} aluminum, 1.5 mL of ECR solution, and 5 mL of sodium acetate solution were mixed together, which could make aluminum-eriochrome cyanine red complex, Al-ECR [36]. The blank solution was prepared from 30 mL of

ultrapure water, 1.5 mL of ECR solution, and 5 mL of sodium acetate solution. The maximum absorbance wavelength of standard solution of 10 mg L^{-1} aluminum was determined against the blank solution from 190 to 800 nm. The calibration curve was prepared using standard solution concentrations (1.5, 2.0, 2.5, 3.0, 3.5, 4.0, 4.5, and 5.0 mg L^{-1} aluminum) and the respective absorbance values. The absorbance of each standard solution concentration was determined at fixed wavelength of 202 nm. Then, the extracted aluminum content in the solution was determined from the calibration curve. The extracted aluminum percentage (% w/w) in solution was determined with respect to the aluminum content present in the kaolinite samples, as given in the following equation:

$$Z = \left(\frac{Z_f}{Z_o}\right) \times 100\%, \quad (4)$$

where Z is the extracted aluminum percentage (% w/w), Z_f is the extracted aluminum (g), and Z_o is the aluminum content in the kaolinite samples (g).

2.4. Statistical Analysis, Model Selection, and Optimization Methods. The statistical analysis, model selection, and optimization were carried out using response surface methodology with central composite design (RSM-CCD). The statistical values were determined using the Design Expert software (Design Expert 10.0.1, trial version). The response surface quadratic models for both the degree of conversion of kaolinite dehydroxylation reaction and extraction yield of aluminum were given in equations (5) and (6), respectively. The analysis of variance (ANOVA) surface quadratic model was conducted for calcination parameters optimization to maximize the responses (degree of conversion of kaolinite dehydroxylation reaction and extracted aluminum). The validation experiments were carried out with triplicates to verify reproducibility of the data and the predicted values.

$$Y = \beta_o + \sum_{i=}^{3} \beta_i x_i + \sum_{i=1}^{2} \sum_{j=i+1}^{3} \beta_{ij} x_i x_j + \sum_{i=1}^{3} \beta_{ii} x_i^2, \quad (5)$$

$$Z = \beta_o + \sum_{i=}^{3} \beta_i x_i + \sum_{i=1}^{2} \sum_{j=i+1}^{3} \beta_{ij} x_i x_j + \sum_{i=1}^{3} \beta_{ii} x_i^2, \quad (6)$$

where Y is the kaolinite dehydroxylation reaction degree of conversion, Z is the extracted aluminum percentage (% w/w), β_o is the value of fixed response at the center point of the design, β_i, β_j, and β_{ij} are the linear, interaction, and quadratic coefficients, respectively, and X_i and X_j are the independent factors in coded values.

3. Results and Discussion

3.1. XRF Analysis of Kaolinite. Table 2 provides the chemical compositions of Ethiopian kaolinite. As given in Table 2, the chemical compositions of Ethiopian kaolinite were mainly silicon oxide (55.76% w/w), aluminum oxide (32.02% w/w), and loss on ignition (11.17% w/w). The results of chemical composition of the present study showed that the Ethiopian kaolinite could be the potential sources of aluminum extraction.

3.2. XRD Analysis of Kaolinite, Metakaolinite, and Extracted Aluminum. Figure 1 shows the XRD analysis of kaolinite, metakaolinite (calcined kaolinite), and extracted aluminum samples. The high intensity peaks of the kaolinite samples were detected at 12.02, 20.61, 24.56, 35.69, 38.65, 55.28, and 63.17° of 2θ angles with the Miller indices of (001), (200), $(\overline{1}10)$, $(\overline{1}31)$, (003), (240), and $(\overline{3}23)$, respectively, as shown in Figure 1(a). The highest intensity XRD peak of the kaolinite samples was observed at the 2θ angle of 12.02°. The crystal pattern of the kaolinite was the monoclinic space group. The crystal pattern unit cell axes were $a = 5.148$ Å, $b = 8.920$ Å, and $c = 14.535$ Å, and angles of $a = 90°$, $\beta = 100.2°$, and $\gamma = 90°$. In addition, the highest intensity of quartz peaks was also observed at 21.03 and 26.28° of 2θ angles. Figure 1(b) shows the XRD reflections of the calcined kaolinite samples at 650 and 700°C. The XRD reflections of the calcined kaolinite samples at 650 and 700°C were amorphous structures. The red and black color XRD curves correspond to the calcined kaolinite samples at 650 and 700°C, respectively. The peaks intensity of calcined kaolinite at 700°C was less than the peaks intensity of calcined kaolinite at 650°C, which indicated that kaolinite samples were transformed to metakaolinite and degree of conversion of dehydroxylation reaction was higher at 700°C than 650°C. The XRD reflections of calcined kaolinite at 650 and 700°C were amorphous structures with the presence of quartz peaks. At 650 and 700°C, highest intensity XRD reflection peaks were obtained at 26.28°, which indicated that quartz was survived during calcination. The quartz peaks were detected at the 2θ angles of 21.03, 26.28, 35.42, 47.19, and 50.76° with Miller indices of (100), (101), (110), (201), and (123), respectively. The kaolinite and calcined kaolinite samples' XRD reflections were crystalline and amorphous, respectively. The crystalline peaks of calcined kaolinite samples vanished, which revealed that amorphous metakaolinite was formed during calcination of kaolinite. This result was in agreement with previous studies [6,22]. Figure 1(c) shows the XRD reflections, crystal system, crystal unit cells, angles, and miller indices of extracted aluminum samples. The extracted aluminum samples crystal system was trigonal (the unit cells were $a = b = c = 7.85$ Å, and the angles were $\alpha = \beta = \gamma = 97°$). The crystal system miller indices were (110), (012), (300), (211), (220), (312), (232), (134), (400), (422), and (511) at the 2θ angles of 15.10, 17.34, 24.19, 27.36, 30.52, 35.01, 39.10, 44.24, 46.88, 63.22, and 69.28°, respectively. Figure 1(d) shows the XRD reflections of standard aluminum chloride hexahydrate for comparison. The standard aluminum chloride hexahydrate crystal system was trigonal (the unit cells were $a = b = c = 7.85$ Å, and the angles were $\alpha = \beta = \gamma = 97°$). The crystal system miller indices were (110), (012), (300), (122), (220), (312), (232), (134), (004), (422), and (511) at the 2θ angles of 15.11, 17.20, 24.32, 27.36, 30.40, 35.14, 39.36, 44.24, 52.14, 63.09, and 69.55°, respectively. The extracted aluminum and the standard

Table 2: Chemical composition of Ethiopian kaolinite.

Oxides	SiO_2	Al_2O_3	TiO_2	K_2O	Na_2O	NaCl	MgO	FeO	LOI*
Chemical composition (% w/w)	55.76	32.02	0.34	0.24	0.13	0.14	0.17	0.03	11.17

LOI*, loss on ignition (determined from TGA analysis).

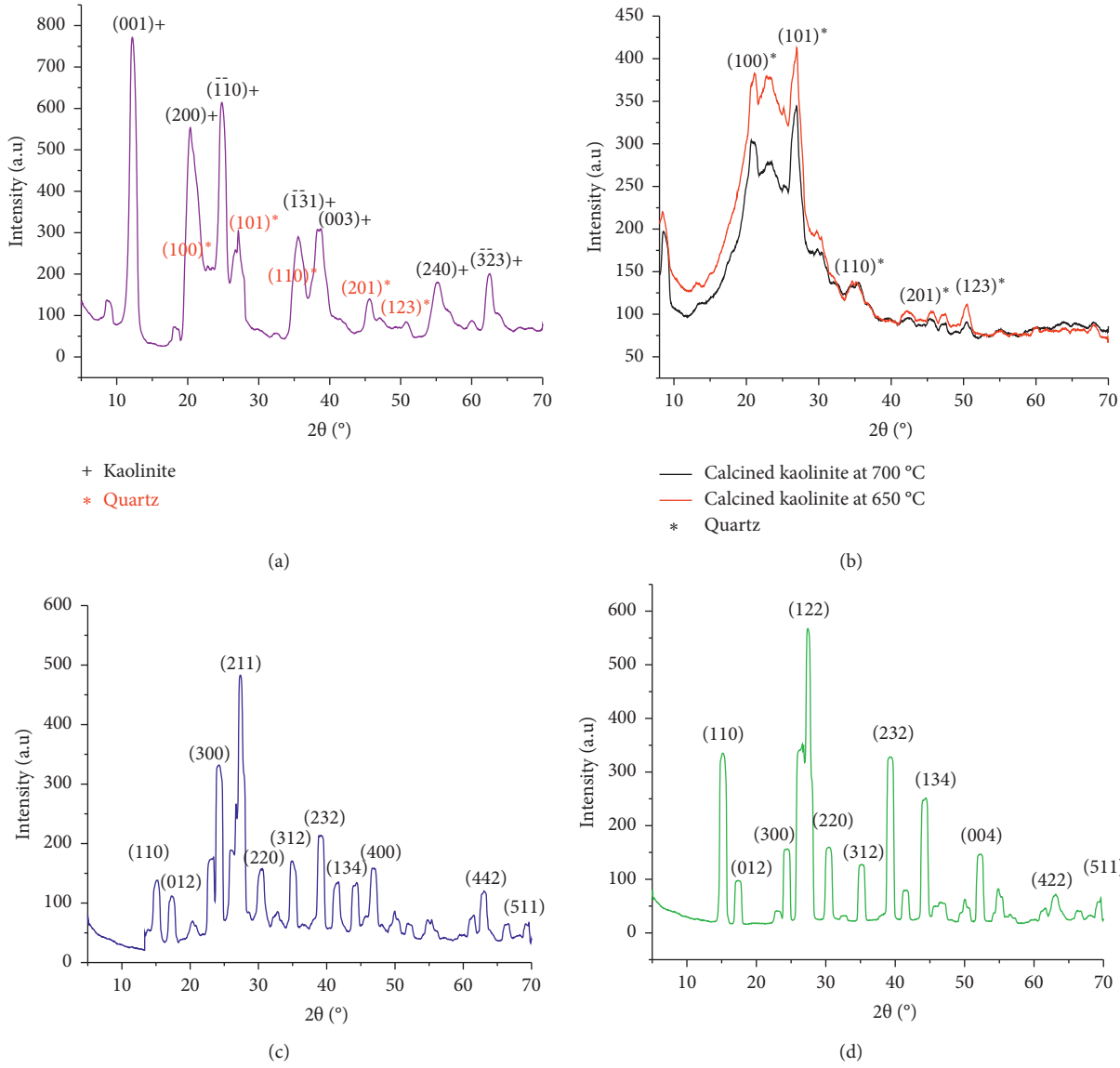

Figure 1: XRD reflections of (a) kaolinite, (b) calcined kaolinite at 650°C and 700°C, (c) extracted aluminum at 700°C, 180 min, and 106 μm, and (d) standard aluminum chloride hexahydrate.

aluminum chloride hexahydrate samples showed the same crystalline structures, which revealed that the extracted aluminum samples were in the form of aluminum chloride hexahydrate.

3.3. FTIR Analysis of Kaolinite, Metakaolinite, and Extracted Aluminum. Figure 2 shows the FTIR curves. Figures 2(a)–2(d) show the FTIR curves of the kaolinite and calcined kaolinite samples at 600, 650, and 700°C, and Figures 2(e) and 2(f) show the FTIR curves of the extracted aluminum and standard aluminum chloride hexahydrate samples. Figure 2(a) shows the FTIR curve of the kaolinite samples. The characteristic bands at 3687 and 3621 cm^{-1} were the stretching bands of hydroxides in the kaolinite samples. The group band at 1648 cm^{-1} attributed to the stretching and bending of hydration water. The band at 1094 cm^{-1} was due to the stretching vibrations of Si–O–Si, and the band at 797 cm^{-1} was the characteristics of quartz which attributed to O–Si–O bending vibrations. The Al–OH group transitional vibration was detected at 908 cm^{-1}, and the bending of Si–O–Al^{VI} octahedral coordinating vibration band was

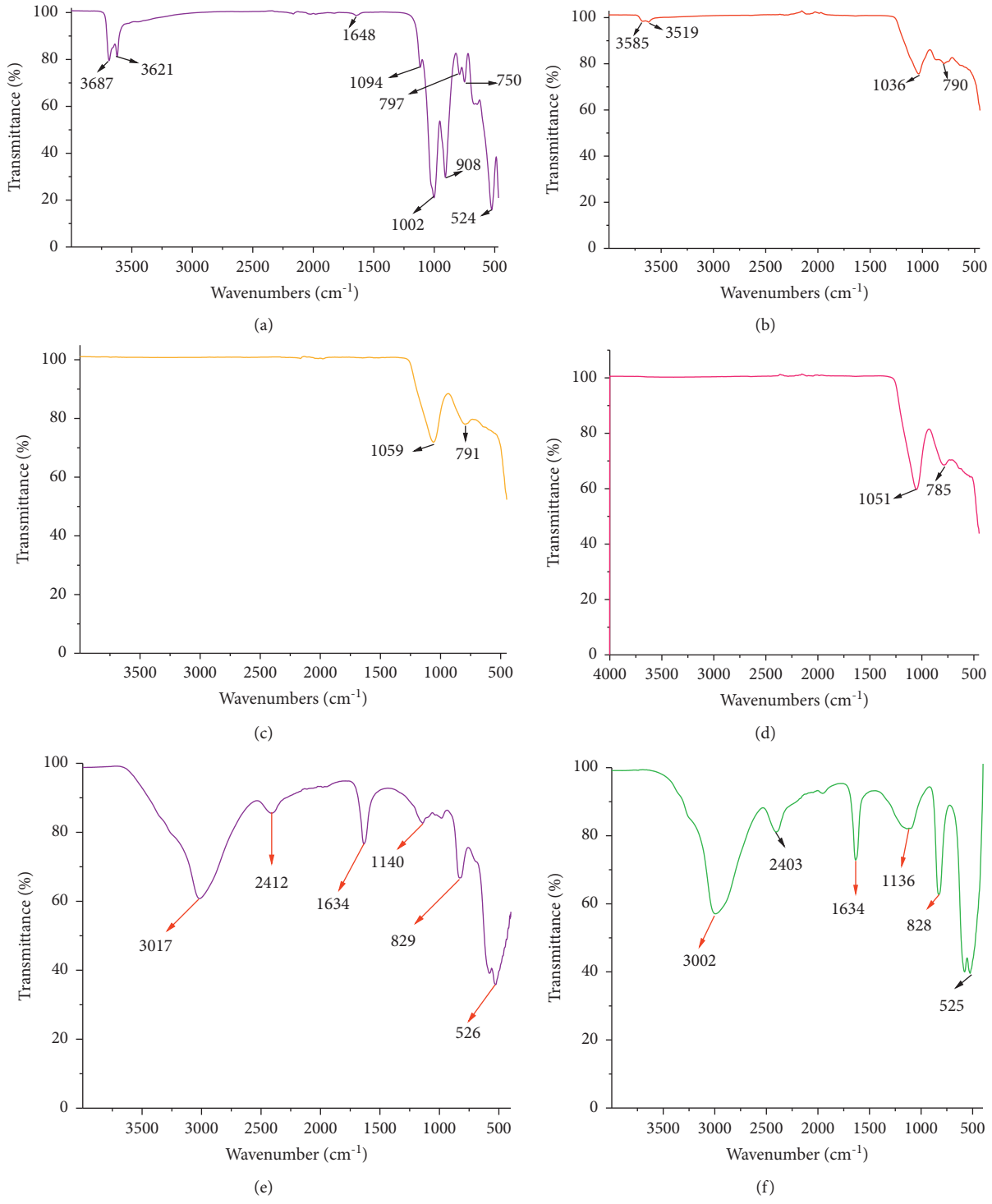

Figure 2: FTIR curves of (a) kaolinite, (b) calcined kaolinite at 600°C, (c) calcined kaolinite at 650°C, (d) calcined kaolinite at 700°C, (e) extracted aluminum at 700°C, 180 min, and 106 μm, and (f) standard aluminum chloride hexahydrate.

obtained at 524 cm^{-1}. Figure 2(b) shows the FTIR curve of the calcined kaolinite samples at 600°C. The hydroxide bands at 3585 and 3519 cm^{-1} were observed for calcined kaolinite samples at 600°C, but the intensity of hydroxide bands was less than the kaolinite samples, which revealed that the kaolinite was partially converted to metakaolinite at 600°C. The bands at 1036 and 790 cm^{-1} were also survived, which attributed to Si–O–Si bending vibrations and O–Si–O bending vibrations. On the other hand, the characteristics bands of the Al–OH group transitional vibration band at 908 cm^{-1} and the bending of Si–O–Al^{VI} octahedral coordinating vibration band at 524 cm^{-1} disappeared due to dehydroxylation reaction during kaolinite calcination. Figure 2(c) shows the FTIR curve of the calcined kaolinite

samples at 650°C. The hydroxyl bands disappeared from the FTIR curve when the kaolinite was calcined at 650°C, which revealed that the kaolinite was transformed into metakaolinite. The characteristics bands of the Al–OH group transitional vibration at 908 cm^{-1} and the bending of $Si–O–Al^{VI}$ octahedral coordinating vibration at 524 cm^{-1} also vanished. In contrast, the bands at 1059 and 791 cm^{-1} were detected which attributed to Si–O–Si bending vibrations and O–Si–O bending vibrations, respectively, at 650°C due to survival of quartz. Figure 2(d) shows the FTIR curve of the calcined kaolinite samples at 700°C. The hydroxide bands disappeared at the calcination temperature of 700°C which confirmed that the kaolinite was transformed into metakaolinite. Furthermore, the Al–OH group transitional vibration at 908 cm^{-1} and the bending of $Si–O–Al^{VI}$ octahedral coordinating vibration at 524 cm^{-1} also vanished. But, the bands at 1051 and 785 cm^{-1} were observed which attributed to O–Si–O bending vibrations due to survival of quartz at 700°C. Thus, the metakaolinite samples were reactive with hydrochloric acid solutions, and the aluminum extraction was maximized at 700°C. In addition, Figure 2(e) shows the FTIR curve of extracted aluminum samples. The function groups' bands were detected at the wavenumbers of 3017, 2412, 1634, 1140, 829, and 526 cm^{-1} which were due to stretching vibration of–OH groups, bending vibration of –OH groups of water molecules, asymmetric stretching vibration of Al–O–Al, bending vibration of Al–OH–Al, and bending vibration of Al–OH, respectively. Figure 2(f) shows the FTIR curve of standard aluminum chloride hexahydrate. The function group bands were obtained at the wavenumbers of 3002, 2403, 1634, 1136, 828, and 525 cm^{-1}, which were due to stretching vibration of –OH groups, bending vibration of –OH groups of water molecules, asymmetric stretching vibration of Al–O–Al, bending vibration of Al–OH–Al, bending vibration of Al–OH, and winding vibration of Al–O, respectively. The extracted aluminum samples showed the same FTIR curves and functional groups bands with the standard aluminum chloride hexahydrate samples, which confirmed that the extracted aluminum samples were in the form of aluminum chloride hexahydrate. Hence, the extracted aluminum chloride hexahydrate might be used to synthesize polyaluminum chloride coagulant for water treatment application.

3.4. DSC Analysis of Kaolinite and Extracted Aluminum. Figure 3 shows the DSC curves and the corresponding specific enthalpy of endothermic peaks. Figures 3(a) and 3(b) show the DSC curves of the kaolinite samples and the specific enthalpy of endothermic peaks, and Figures 3(d)–3(f) show the DSC curves of extracted aluminum and standard aluminum chloride hexahydrate samples and the corresponding specific enthalpy of endothermic peaks. Figure 3(a) shows the DSC curve of the kaolinite samples. In the DSC curve, three endothermic peaks were detected from 25 to 600°C. The first, second, and third endothermic peaks occurred due to adsorbed water removal, impurities decomposition, and dehydroxylation reaction of kaolinite, respectively. The dehydroxylation reaction of kaolinite was observed from 450 to 600°C, which revealed the formation of metakaolinite. Figure 3(b) shows the specific enthalpy of the three endothermic peaks of kaolinite samples DSC curve. The specific enthalpy values due to water dehydration (Δh_w), impurities decomposition (Δh_d), and dehydroxylation reaction of kaolinite (Δh_p) were 103.21, 76.45, and 269.31 J g^{-1}, respectively. In addition, Figure 3(c) shows the DSC curve of the extracted aluminum chloride hexahydrate samples decomposition endothermic peak. The beginning and the completion points of the endothermic peak were detected at 120 and 400°C, respectively. The deep point of the endothermic peak was obtained at 196°C. Figure 3(d) shows the specific enthalpy of the extracted aluminum chloride hexahydrate samples decomposition, which was obtained from endothermic peak area of the DSC curve. The specific enthalpy of the endothermic peak was 158.07 J g^{-1}. Moreover, Figure 3(e) shows the DSC curve of the standard aluminum chloride hexahydrate endothermic peak for comparison. The endothermic peak beginning and ending points were identified at 120 and 400°C, respectively. The deep point of the endothermic peak was also found at 199°C. Figure 3(f) shows the specific enthalpy of the decomposition of standard aluminum chloride hexahydrate. The specific heat of the endothermic peak was 188.44 J g^{-1}. In the DSC analysis, the DSC curves of the extracted aluminum chloride hexahydrate samples and standard aluminum chloride hexahydrate samples had the same endothermic peak, which revealed that the thermal property was the same. The extracted aluminum chloride hexahydrate decomposition specific enthalpy was less than the standard aluminum chloride hexahydrate decomposition, which indicated that extracted aluminum chloride hexahydrate required less energy for decomposition. The extracted aluminum chloride hexahydrate might be suitable for recovery of aluminum oxide at lower energy consumption. The aluminum chloride hexahydrate could be decomposed into aluminum oxide, water vapor, and hydrogen chloride gas. The decomposition temperature and the endothermic peak of extracted aluminum chloride hexahydrate agreed with the results which have been reported [40].

3.5. TGA Analysis of Kaolinite and Extracted Aluminum. Figures 4(a)–4(c) show the TGA and DTA curves of kaolinite, extracted aluminum chloride hexahydrate, and standard aluminum chloride hexahydrate samples, respectively. Figure 4(a) shows the TGA and DTA curves of the kaolinite samples from 25 to 1100°C. The TGA curve shows the mass loss of the kaolinite samples in the thermogravimetry analysis. The mass losses occurred due to impurities decomposition, and dehydroxylation reaction of kaolinite was 11.17%. In the DTA curve, three endothermic peaks and one exothermic peak were detected. In the first endothermic peak, the adsorbed water was removed at the temperature below 100°C. The impurities decomposition was detected from 250 to 300°C, which represented the second endothermic peak, and the mass loss was 1.86%. The third endothermic peak was due to dehydroxylation reaction of kaolinite (formation of metakaolinite) from 450 to 700°C

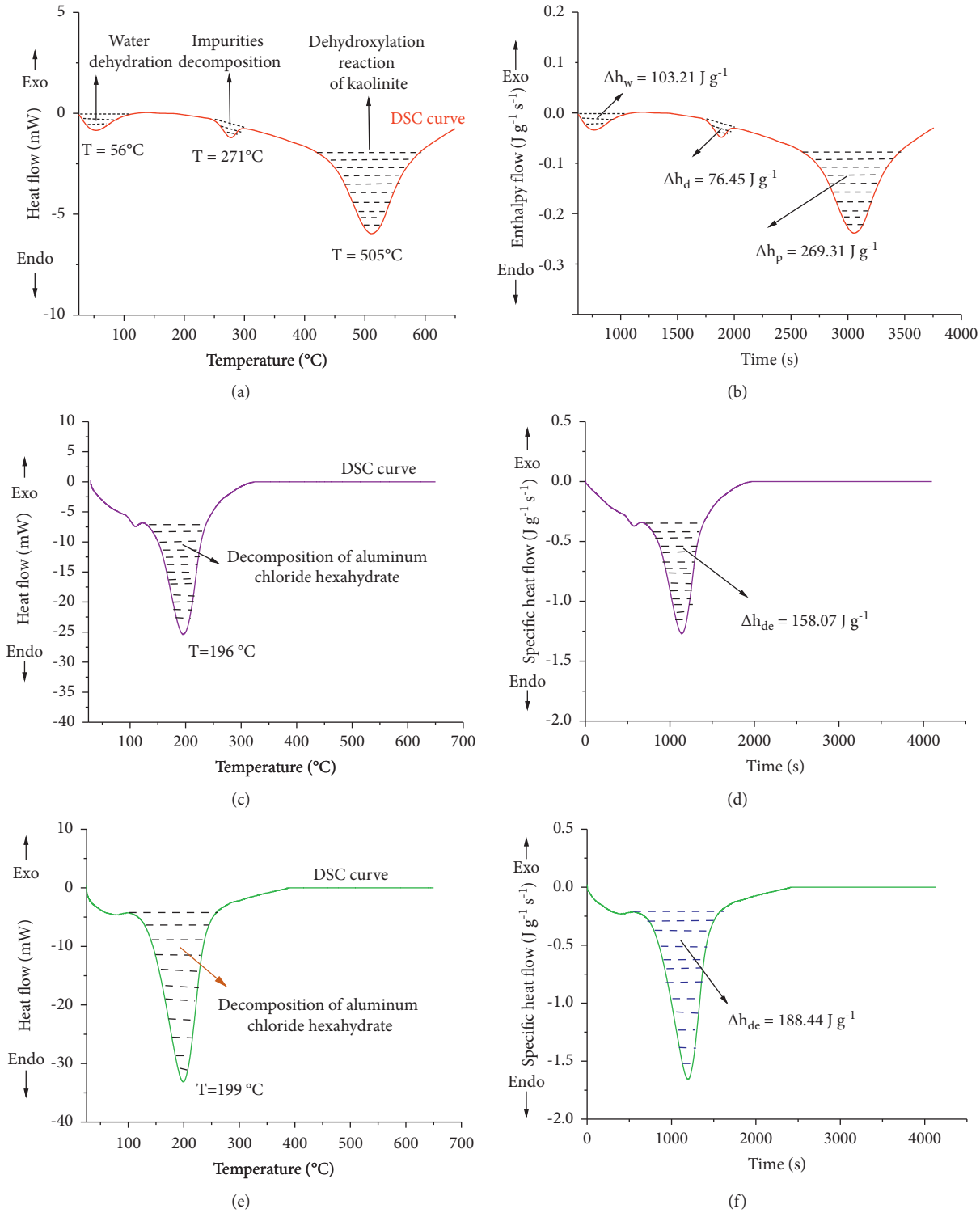

FIGURE 3: DSC curves of (a) kaolinite, (b) specific enthalpy of kaolinite, (c) extracted aluminum at 700°C, 180 min, and 106 μm, (d) specific enthalpy of extracted aluminum at 700°C, 180 min, and 106 μm, (e) standard aluminum chloride hexahydrate, and (f) specific enthalpy of standard aluminum chloride hexahydrate.

with the mass loss of 9.31%. Increasing the heating temperature from 700 to 970°C, mass loss and phase transformation did not occur. The detected endothermic peaks agreed with the results described [37]. Furthermore, the exothermic peak was observed from 970 to 1030°C, which might be caused by phase transformation of amorphous metakaolinite to crystalline spinel. The exothermic peak due to transformation of metakaolinite phase to spinel has been

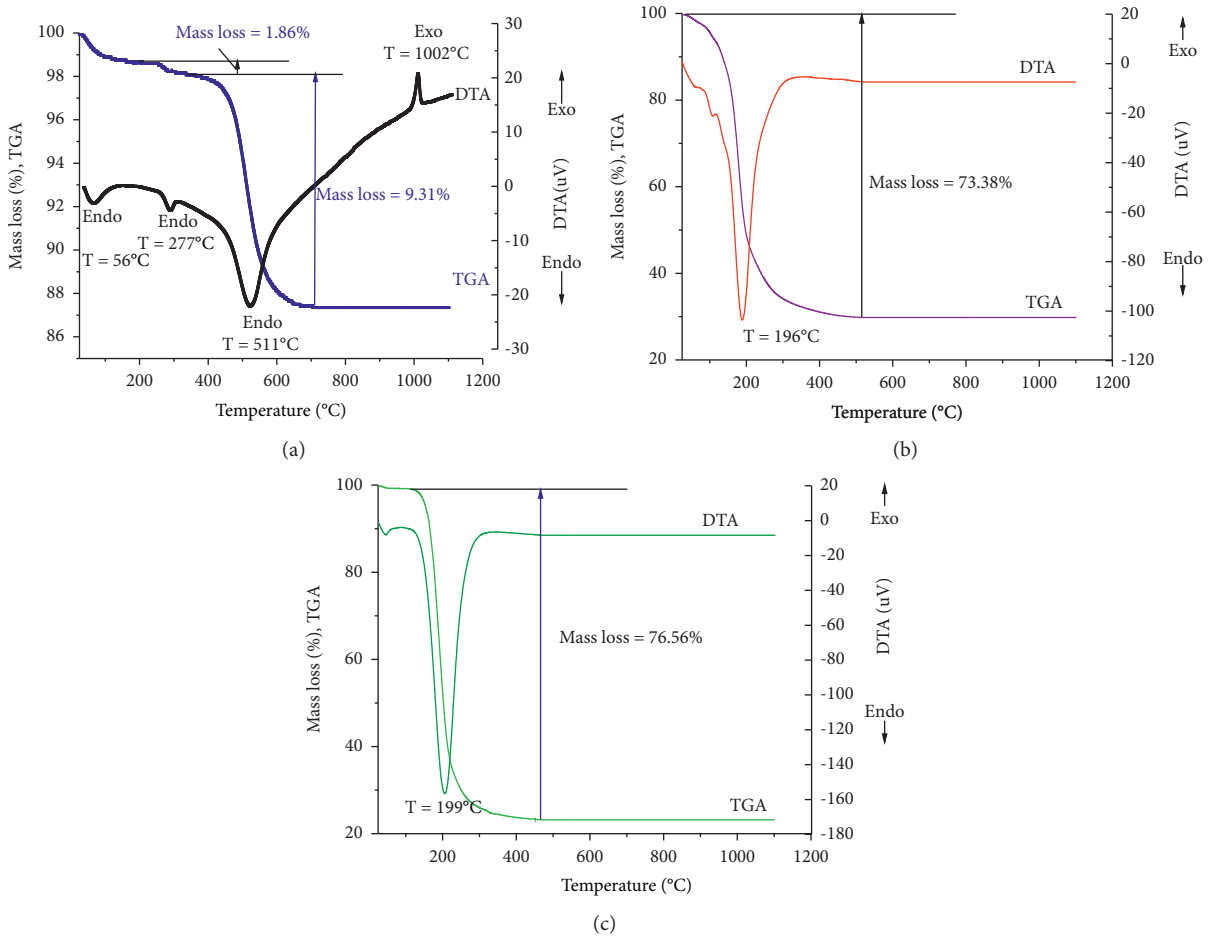

Figure 4: TGA curves of (a) kaolinite, (b) extracted aluminum at 700°C, 180 min, and 106 μm, and (c) standard aluminum chloride hexahydrate.

detected at 985°C [41]. Increasing the calcination temperature over 1050°C, the spinel phase ($Si_3Al_4O_{12}$) has been nucleated and transformed to mullite ($3Al_2O_3$ $2SiO_2$) [42]; however, in this work, formation of mullite was not detected up to 1100°C. Figure 4(b) shows the TGA and DTA curves of extracted aluminum chloride hexahydrate samples mass loss and endothermic peak, respectively. The samples decomposition temperature at the endothermic peak dip point was 196°C, and mass loss was 73.38%. Furthermore, Figure 4(c) shows the TGA and DTA curves of standard aluminum chloride hexahydrate samples mass loss and endothermic peak, correspondingly. The decomposition temperature at the endothermic peak dip point was 199°C, and mass loss was 76.56%. The endothermic peaks, decomposition temperatures, and mass loss of both extracted aluminum chloride hexahydrate and standard aluminum chloride hexahydrate samples were almost the same which revealed that the thermal property of extracted aluminum chloride hexahydrate and standard aluminum chloride hexahydrate samples were the same. The extracted aluminum chloride hexahydrate samples decomposed from 120 to 450°C, which indicated that the aluminum chloride hexahydrate could be used for different applications in the process temperature less than 120°C. In the process temperatures at 120°C and more, the extracted aluminum chloride hexahydrate could be decomposed into aluminum oxide, water vapor, and hydrogen chloride gas [43].

3.6. UV-Vis Analysis of Extracted Aluminum. The maximum absorbance for both the extracted aluminum and the standard aluminum chloride hexahydrate solution samples was detected at 202 nm wavelength as shown in the Supplementary Materials (Figure S1). The standard solutions absorbance versus concentrations calibration plot was carried out from 1.5 to 5.0 mg L^{-1}, and the corresponding absorbance values were from 0.333 to 0.667, respectively. The regression linear equation of absorbance versus concentration of standard solutions is given in equation (7). The extracted aluminum contents in the solution were determined using equation (4). The values of extracted aluminum varied from 63.64 to 71.27% w/w.

$$A = 0.09837C, \tag{7}$$

where A is the absorbance (a.u), and C is the concentration of aluminum (mg L^{-1}).

Table 3: CCD experiments for optimization of calcination parameters on responses: degree of conversion of kaolinite dehydroxylation reaction (Y) and extracted aluminum (Z).

Run	Temperature (°C)	Time (min)	Particles size (μm)	Initial mass, m_o (g)	Final mass, m_f (g)	Y (The dehydroxylation reaction of kaolinite degree of conversion determined from mass loss during calcination of kaolinite samples and TGA LOI value.)	Z (The extracted aluminum content determined from UV-vis standard solutions calibration curve.) (% w/w)
1	600	120	106	15 ± 0.02	13.38 ± 0.02	0.963	66.48
2	565	150	250	15 ± 0.01	13.43 ± 0.01	0.936	63.64
3	650	150	250	15 ± 0.01	13.37 ± 0.01	0.970	70.26
4	650	150	250	15 ± 0.01	13.37 ± 0.01	0.968	70.19
5	700	120	106	15 ± 0.02	13.34 ± 0.01	0.989	70.25
6	650	150	250	15 ± 0.01	13.37 ± 0.01	0.971	70.02
7	700	120	355	15 ± 0.01	13.38 ± 0.02	0.965	66.62
8	650	150	250	15 ± 0.01	13.37 ± 0.01	0.969	70.22
9	734	150	250	15 ± 0.01	13.36 ± 0.01	0.976	68.36
10	700	180	106	15 ± 0.02	13.34 ± 0.01	0.991	71.27
11	600	180	106	15 ± 0.01	13.37 ± 0.01	0.969	67.81
12	650	150	250	15 ± 0.01	13.37 ± 0.01	0.970	70.23
13	600	120	355	15 ± 0.02	13.41 ± 0.01	0.947	64.39
14	650	150	63	15 ± 0.01	13.34 ± 0.01	0.990	71.13
15	700	180	355	15 ± 0.02	13.37 ± 0.01	0.971	67.64
16	650	150	250	15 ± 0.01	13.37 ± 0.02	0.969	70.21
17	650	200	250	15 ± 0.01	13.36 ± 0.01	0.974	69.23
18	600	180	355	15 ± 0.01	13.40 ± 0.01	0.952	65.73
19	650	100	250	15 ± 0.01	13.38 ± 0.02	0.964	67.55
20	650	150	500	15 ± 0.01	13.39 ± 0.02	0.961	63.83

3.7. Degree of Conversion and Extracted Aluminum Analysis. The degree of conversion of kaolinite dehydroxylation reaction and extracted aluminum results were determined at various calcination conditions. Table 3 provides the degree of conversion of kaolinite dehydroxylation reaction and extracted aluminum values at different calcination conditions. The degree of conversion of kaolinite dehydroxylation reaction increased as the calcination temperature and time increased, and the particles size was reduced. The degree of conversion of kaolinite dehydroxylation reaction varied from 0.936 to 0.991. The extracted aluminum values also increased as the calcination temperature and time increased, and the particles size was reduced. The values of extracted aluminum varied from 63.64 to 71.27% w/w. The maximum values of both degree of conversion of kaolinite dehydroxylation reaction and extracted aluminum were obtained at 700°C, 180 min, and 106 μm. However, the minimum values of both degree of conversion of kaolinite dehydroxylation reaction and extracted aluminum were determined at 565°C, 150 min, and 250 μm for the calcination temperature, time, and particles size, respectively. Thus, the maximum degree of conversion of kaolinite dehydroxylation reaction and extracted aluminum values were 0.991 and 71.27% w/w, respectively, at 700°C, 180 min, and 106 μm.

3.8. Statistical Analysis, Model Selection, and Optimization for Degree of Conversion

3.8.1. Statistical Analysis and Model Selection for Degree of Conversion. Table 4 provides the summary of lack of fit and statistical analysis in model selection for degree of conversion of kaolinite dehydroxylation reaction. On the basis of the statistical analysis, the response surface quadratic model was selected. The quadratic model lack of fit value was not significant, and the correlation coefficient (R^2) adjusted correlation coefficient (Adj. R^2) and the predicted correlation coefficient (pre. R^2) values were 0.994, 0.990 and 0.968, respectively. The adequate precision (AP) and the coefficient of variance (CV) values were also 59.03 and 0.41%, respectively, which confirmed that the quadratic model could be used to navigate the design space of the response values and experimental data could be reproducible. The quadratic model of standard deviation (SD) and predicted residual sum of squares (PRESS) values were less than the linear and the 2-factor interactions (2FI) models of SD and PRESS values by five folds. The cubic and higher order models were aliased. The details of statistical analysis for model selection are given in supplementary materials (Table S1). Hence, the response values were well described by response surface quadratic model, which was selected as the best model for analysis of variance and optimization.

3.8.2. Quadratic Model Analysis of Variance for Degree of Conversion. Table 5 provides the analysis of variance (ANOVA) for the response surface quadratic model. The model F value was 212.40 and the p value was less than 0.0001, which indicated that the quadratic model was significant. The quadratic model lack of fit test' F value of 2.22 also indicated that the lack of fit was not significant relative to the pure error. The linear effects of temperature (X_1), time (X_2), and particles size (X_3), the interactions effect of temperature and particles size (X_1X_3), and the quadratic

Table 4: Summary of lack of fit and statistical analysis in model selection for degree of conversion of kaolinite dehydroxylation reaction.

Source	Sequential p value	Lack of fit p value	Adj. R^2	Pred. R^2
Linear	<0.0001	0.0003	0.8135	0.7101
2 FI	0.9396	0.0002	0.7773	0.6871
Quadratic	<0.0001	0.2011	0.9901	0.9685
Cubic (cubic model was aliased for dehydroxylation reaction of kaolinite samples degree of conversion)	0.2011		0.9939	

Table 5: ANOVA for surface quadratic model (response: degree of conversion of kaolinite dehydroxylation reaction).

Source	Sum of squares	Df	Mean square	F value	P value	
Model	3.384×10^{-3}	9	3.760×10^{-3}	212.40	<0.0001	Significant
X_1, temperature	1.024×10^{-3}	1	1.024×10^{-3}	578.72	<0.0001	Significant
X_2, time	7.560×10^{-5}	1	7.560×10^{-5}	42.71	<0.0001	Significant
X_3, particles size	4.950×10^{-4}	1	4.950×10^{-4}	279.61	<0.0001	Significant
X_1X_2	1.125×10^{-6}	1	1.125×10^{-6}	0.64	0.4439	Not significant
X_1X_3	1.343×10^{-5}	1	1.343×10^{-5}	7.59	0.0203	Significant
X_2X_3	1.365×10^{-6}	1	1.365×10^{-6}	0.77	0.4005	Not significant
X_1^2	3.346×10^{-4}	1	3.346×10^{-4}	189.00	<0.0001	Significant
X_2^2	1.094×10^{-6}	1	1.094×10^{-6}	0.62	0.4500	Not significant
X_3^2	1.183×10^{-4}	1	$1.183.110^{-4}$	66.83	<0.0001	Significant
Residual	1.770×10^{-5}	10	1.770×10^{-6}			
Lack of fit	1.220×10^{-5}	5	2.441×10^{-6}	2.22	0.2011	Not significant
Pure error	5.500×10^{-6}	5	1.100×10^{-6}			
Cor total SS	3.402×10^{-3}	19				

effects of temperature (X_1^2) and particles size (X_3^2) were significant terms. The variance inflation factor (VIF) values of significant terms in the model were from 1.02 to 1.45, which revealed that the associated independent variable was moderately collinear with other variables in the model. The quadratic model regression coefficient estimates, standard error, 95% CI, and VIF values for degree of conversion are given in Supplementary Materials (Table S2). The positive signs of the coefficients of X_1 and X_2 revealed that the degree of conversion increased, while calcination temperature and time were linearly increased. The negative sign of coefficient of X_3 described that the degree of conversion increased, while the particles size was linearly decreased. The coefficient of X_1X_3 was negative, which indicated that the degree of conversion was negatively affected by the interaction of temperature and particles size. The negative sign of the quadratic effect of temperature was in contrast with the linear effect of temperature, which revealed that the degree of conversion reached at the optimum value and then after the degree of conversion might be declined, while the temperature was increased with quadratic order. The insignificant terms (X_1X_2, X_2X_3, and X_2^2) in the quadratic model were discarded to improve the model. The final equation of the quadratic model response values in terms of coded factors is expressed by the following equation:

$$\begin{aligned} Y = {} & 0.97 + 0.010X_1 + 2.844 \times 10^{-3}X_2 - 0.011X_3 \\ & - 2.040 \times 10^{-3}X_1X_3 \\ & - 4.789 \times 10^{-3}X_1^2 - 6.166 \times 10^{-3}X_3^2, \end{aligned} \quad (8)$$

where Y is the degree of conversion of kaolinite dehydroxylation reaction, X_1 is the temperature, X_2 is the time, and X_3 is the particles size.

3.8.3. Diagnostics Analysis of the Quadratic Model for Degree of Conversion. In the outliers' analysis of the response values, the normal probability versus residuals plot followed normal distribution along the straight line, and the observation with internally and externally studentized residuals values were less than the absolute value of 3.0 and 4.0, respectively; the result indicated that the outlier was not obtained in the response values. The internally and externally studentized residuals versus the predicted response values plot were a random scatter with a constant range of residuals across the graph. The scatter plot of the actual response values versus predicted response values were evenly laid on the 45° straight line which confirmed that the predicted response values could be easily predicted by the quadratic model. Furthermore, in the Box–Cox plot of lambda versus residual sum of squares, the ratio of maximum response value to minimum response value was 1.06, which confirmed that a power transformation was not required to improve the quadratic model. The diagnostics analysis plots are given in Supplementary Materials (Figure S2).

3.8.4. The Quadratic Model Graphs Analysis for Degree of Conversion. For the response surface quadratic model graphs analysis of kaolinite calcination conditions, Figures 5(a)–5(d) show the perturbation plot and the surface plots of the effects of the calcination factors on the degree of conversion of kaolinite dehydroxylation reaction. Figure 5(a) shows the perturbation plot of the effect of factors on degree of conversion. The calcination time curve was comparatively flat, which confirmed that the degree of conversion of kaolinite dehydroxylation reaction was less sensitive for the calcination time. On the other hand, the

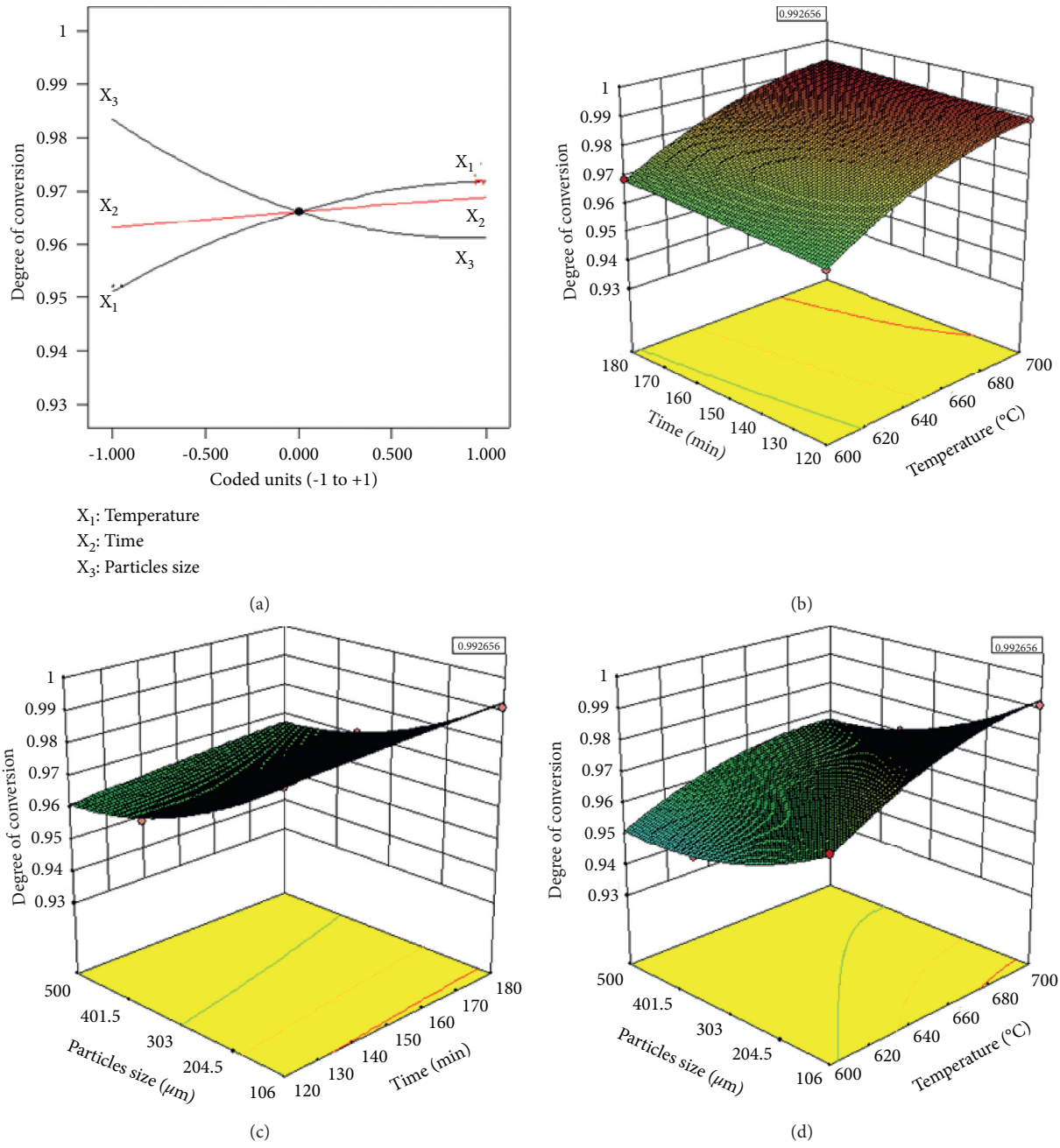

Figure 5: Model graphs of (a) perturbation plot of the factors effect on degree of conversion, (b) the surface plot of calcination temperature and time effect, (c) the surface plot of calcination time and particles size effect, and (d) the surface plot of calcination temperature and particles size effect on degree of conversion.

calcination temperature and particle size curves were steep slope and curvature, which indicated that the degree of conversion of kaolinite dehydroxylation reaction was more affected by both temperature and particles size. Figure 5(b) shows the surface plot of the effects of calcination temperature and time on the degree of conversion. The degree of conversion of kaolinite dehydroxylation reaction increased up to 0.991, while both calcination temperature and time increased to 700°C and 180 min, respectively. Figure 5(c) shows the surface plot of the effect of calcination time and particles size on the degree of conversion of kaolinite dehydroxylation reaction. As the calcination time was increased to 180 min and the particles size was reduced upto106 μm, the degree of conversion of kaolinite dehydroxylation reaction improved up to 0.991. Figure 5(d) shows the effect of the calcination temperature and particles size on the degree of conversion. The degree of conversion of kaolinite dehydroxylation reaction enhanced up to 0.991, when calcination temperature was increased to 700°C and particles size was reduced to 106 μm.

3.9. Statistical Analysis, Model Selection, and Optimization for Extracted Aluminum

3.9.1. Statistical Analysis and Model Selection for Extracted of Aluminum. Table 6 provides the lack of fit and statistical analysis values summary in model selection for extracted aluminum. The quadratic model lack of the fit value was not significant, and the R^2, Adj. R^2, and pred. R^2 values were 0.999, 0.998, and 0.996, respectively. The CV and AP values were also 0.13% and 118.06, respectively, which confirmed that the response values could be reproducible. In contrast, the linear and 2FI models' lack of fit values were significant, and the Adj. R^2 and the pred. R^2 values were less than 0.55, which revealed that the linear and 2FI models were unable to describe the response values. In addition, the cubic model and higher orders were aliased. The statistical analysis summary for model selection is given in Supplementary Materials (Table S3). Therefore, the response values were well represented by the quadratic model, which was selected as the best model for analysis of variance and optimization.

3.9.2. The Quadratic Model Analysis of Variance for Extracted Aluminum. The quadratic model analysis of variance (ANOVA) for extracted aluminum is given in Table 7. The model F value was 1495.52, and the p value was less than 0.0001 which indicated that the quadratic model was significant. The quadratic model lack of fit test' F value of 1.30 also indicated that the lack of fit was not significant relative to the pure error. The linear effects of temperature (X_1), time (X_2), and particles size (X_3), the interactions effect of temperature and time (X_1X_2), temperature and particles size (X_1X_3), and the quadratic effects of temperature (X_1^2), time (X_2^2), and particles size (X_3^2) were significant terms in the quadratic model. The variance inflation factor (VIF) values of significant terms in the model were from 1.02 to 1.45, which revealed that the associated independent factor was moderately collinear with other factors in the quadratic model. Moreover, the response values at the design center point between 95% CI low and 95% CI high were 69.27% w/w and 69.43% w/w, respectively, which indicated that the average value of the response was determined at the specified setting. The regression coefficient estimates, standard error, 95% CI, and VIF values for extracted aluminum is shown in Supplementary Materials (Table S4). The positive signs of the coefficients of X_1 and X_2 revealed that extracted aluminum values increased, while calcination temperature and time were linearly increased. But, the negative sign of the coefficient of X_3 described that extracted aluminum values increased while the particles size was linearly decreased. The values of extracted aluminum reduced, while the interactions of temperature with time and temperature with particles size were increased. The signs of the quadratic effects of calcination temperature, time, and particles size were all negative, which confirmed that the values of extracted aluminum reached the optimum value, while the calcination temperature and time increased, and particles size was reduced with quadratic order. The highest and lowest effects on the response values occurred due to the particles size and time, respectively. The insignificant term (X_2X_3) in the quadratic model was discarded to improve the model. The final equation of the quadratic model in terms of coded factors is expressed by the following equation:

$$\begin{aligned} Z = {} & 69.35 + 1.20X_1 + 0.55X_2 - 3.66X_3 \\ & - 0.079X_1X_2 - 0.61X_1X_3 \\ & - 1.48X_1^2 - 0.66X_2^2 - 1.87X_3^2, \end{aligned} \tag{9}$$

where Z is the extracted aluminum (% w/w), X_1 is the temperature, X_2 is the time, and X_3 is the particles size.

3.9.3. The Diagnostics Analysis of the Quadratic Model for Extracted Aluminum. In the diagnostics analysis of the response values, internally and externally studentized residuals versus the normal probability plots followed normal distribution along the straight line, which indicated that the outliers' were not obtained in the response values. The internally and externally studentized residuals versus the predicted response values plots were also a random scatter with a constant range of residuals across the graph, and the studentized residuals values were less than the absolute value of 3.0 and 4.0, respectively. In addition, the scatter plot of the actual response values versus predicted response values evenly laid on the 45° straight line which confirmed that the predicted response values could be easily predicted by the quadratic model. The Box–Cox plot of residual sum of squares analysis also confirmed that a power transformation was not required to improve the quadratic model, since the extracted aluminum maximum value to minimum value ratio was 1.12, which was less than 3.0. The response values diagnostics analysis plots are given in Supplementary Materials (Figure S3).

3.9.4. The Quadratic Model Graphs Analysis for Extracted Aluminum. Figures 6(a)–6(d) show the perturbation plot and the surface plots of the effects of factors on extracted aluminum values. Figure 6(a) shows the perturbation plot of the effect of factors on extracted aluminum. The calcination temperature and particles size curves were steep slope and curvature, which revealed that the extracted aluminum values were more sensitive for both calcination temperature and particles size. Instead, the calcination time curve was relatively flat line, which confirmed that extracted aluminum values were less sensitive for the calcination time. In surface plot analysis, Figure 6(b) shows the surface plot of the effects of calcination temperature and time on extracted aluminum values. The extracted aluminum increased, while both calcination temperature and time were increased. The extracted aluminum maximum values was 71.27% w/w at 700°C and 180 min; and the minimum value was 63.64% w/w at 565°C and 150 min. Figure 6(c) shows the surface plot of the effect of the calcination time and particles size on the values of extracted aluminum. The extracted aluminum increased to 71.27% w/w as the calcination time increased to 180 min, and the particles size was reduced to106 μm. Figure 6(d) shows the effect of calcination temperature and particles size on extracted aluminum values.

Table 6: Summary of lack of fit and statistical analysis in model selection for extracted aluminum.

Source	Sequential p value	Lack of fit p value	Adj. R^2	Pred. R^2
Linear	0.0012	<0.0001	0.5478	0.4469
2 FI	0.9422	<0.0001	0.4593	0.0078
Quadratic	<0.0001	0.3889	0.9986	0.9965
Cubic (cubic model was aliased conversion for extracted aluminum)	0.3889		0.9988	

Table 7: ANOVA for the surface quadratic model (response: extracted aluminum).

Source	Sum of squares	Df	Mean square	F value	P value Prob > F	Remark
Model	113.77	9	12.64	1495.52	<0.0001	Significant
X_1, temperature	13.56	1	13.56	1604.31	<0.0001	Significant
X_2, time	2.85	1	2.85	336.77	<0.0001	Significant
X_3, particles size	53.71	1	53.71	6354.20	<0.0001	Significant
X_1X_2	0.050	1	0.050	5.87	0.0359	Significant
X_1X_3	1.20	1	1.20	142.36	<0.0001	Significant
X_2X_3	1.391×10^{-4}	1	1.391×10^{-4}	0.016	0.9005	Not significant
X_1^2	31.86	1	31.86	3769.00	<0.0001	Significant
X_2^2	6.15	1	6.15	728.12	<0.0001	Significant
X_3^2	10.86	1	10.86	1285.11	<0.0001	Significant
Residual	0.085	10	8.452×10^{-3}			
Lack of fit	0.048	5	9.568×10^{-3}	1.30	0.3889	Not significant
Pure error	0.037	5	7.337×10^{-3}			
Cor total SS	113.85	19				

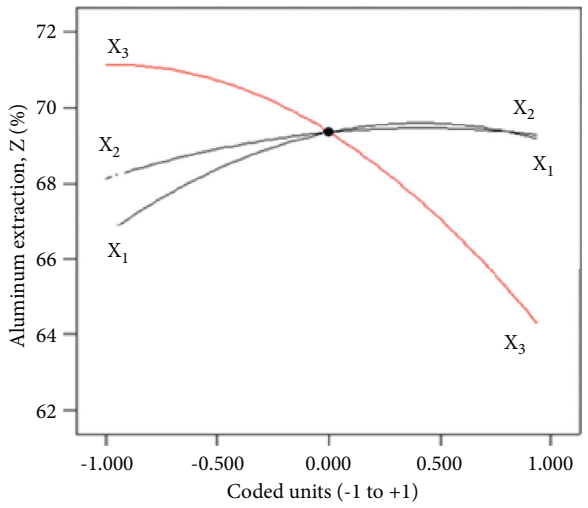

X_1: Temperature
X_2: Time
X_3: Particles size

(a)

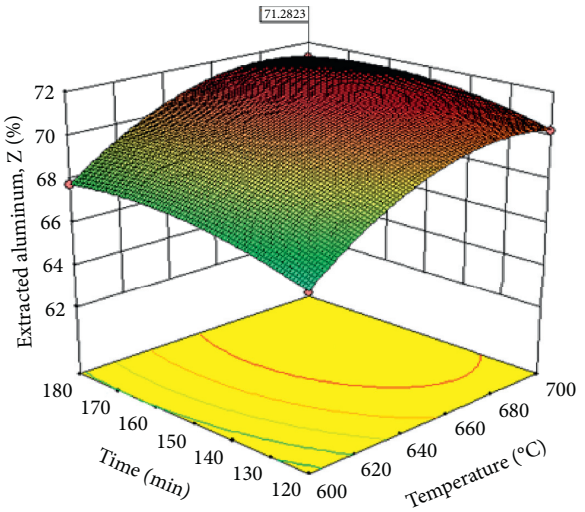

(b)

Figure 6: Continued.

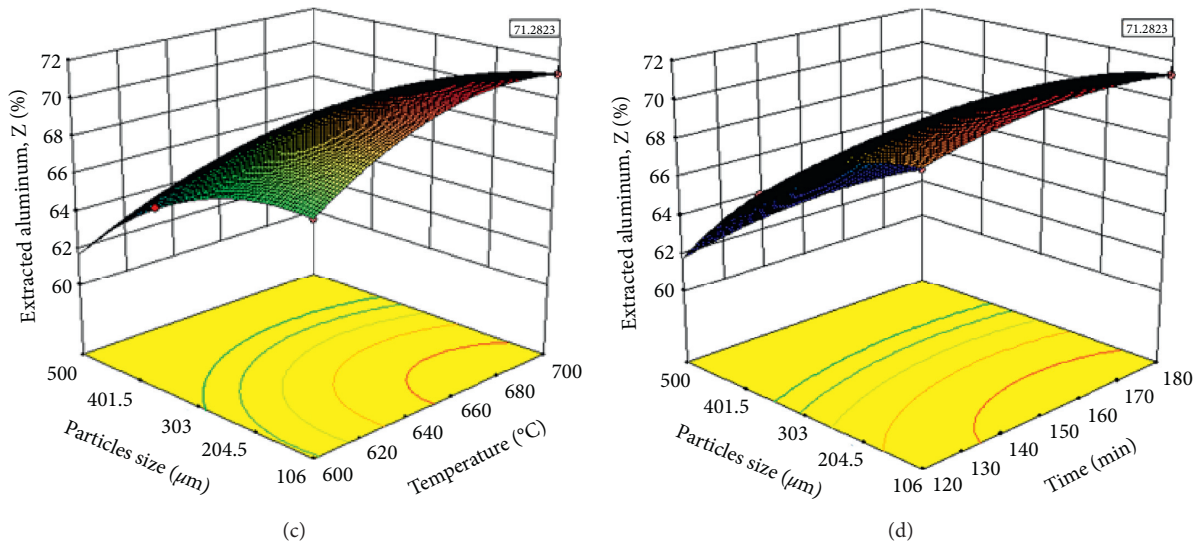

Figure 6: Model graphs of (a) perturbation plot of calcination temperature, time, and particles size on extracted aluminum, (b) the surface plot of calcination temperature and time effect, (c) the surface plot of calcination time and particles size effect, and (d) the surface plot of calcination temperature and particles size effect on extracted aluminum.

Table 8: Comparison of the present study with various literature.

Origin of kaolinite	Optimum calcination conditions	Extraction yield of aluminum (% w/w)	References
Nigerian	600°C, 60 min, and 300 μm	50.27	[21]
Saudi Arabian	600°C, 60 min, and 149 μm	63	[25]
Iraqi	700°C, 120 min, and 125 μm	70	[19]
Chinese	800°C, 180 min, and 44 μm	98.7	[20]
Egyptian	850°C, 120 min, and 90 μm	75	[26]
Egyptian	700°C and 120 min	81.33	[44]
Jordanian	700°C, 180 min, and 75 μm	79.28	[45]
Ethiopian	700°C, 180 min, and 106 μm	71.28	This study

As the calcination temperature was increased to 700°C and the particles size was reduced to 106 μm, the values of extracted aluminum increased to 71.27% w/w.

3.10. Optimum Predicted Calcination Conditions and Experimental Verification. The optimum values of both the degree of conversion of kaolinite dehydroxylation reaction and the extracted aluminum were predicted as 0.992 and 71.28% w/w, respectively, at the optimum calcination conditions of 700°C, 180 min, and 106 μm with desirability of 1.00. The desirability plot of optimum calcination conditions and optimum values of degree of conversion and extracted aluminum is shown in Supplementary Materials (Figure S4). The validation experiment values of degree of conversion of kaolinite dehydroxylation reaction and extracted aluminum were 0.99 and 71.10% w/w, respectively. The results revealed that the validation experiment values were identical as the predicted response values; plus, the generated quadratic model was appropriate to predict the response values.

3.11. Comparison of the Present Study with Various Literature. Table 8 provides the comparison of this study with various literature reports. The calcination conditions of kaolinite from various origins showed different extraction yields of aluminum. The extraction yields of aluminum from Nigerian [21], Saudi Arabian [25], and Iraqi [19] kaolinite have been 50.27, 63 and 70% w/w, respectively, which indicated that better extraction yield of aluminum was obtained in this study over those previously published reports. However, the extraction yields of aluminum from Chinese [20], Egyptian [26,44], and Jordanian [45] kaolinite have been 98.7, 75,81.33, and 79.28% w/w, respectively, which confirmed that relatively higher extraction yield of aluminum was obtained as compared to this study. The difference in the extraction yield of aluminum from various origins of kaolinite in the previous and present studies might be due to variation of geographical location of kaolinite sources, calcination, and extraction process parameters.

4. Conclusion

The crystalline kaolinite was transformed into amorphous metakaolinite during calcination. The extracted aluminum was in the form of aluminum chloride hexahydrate crystals, and the crystals system was trigonal. In the thermal analysis of extracted aluminum chloride hexahydrate, one endothermic peak was detected due decomposition reaction of

aluminum chloride hexahydrate into aluminum oxide, water vapor, and hydrogen chloride gas. The aluminum chloride hexahydrate was decomposed from 120 to 450°C, and the mass loss due to decomposition was 73.38% w/w. The specific heat of extracted aluminum chloride hexahydrate samples' decomposition endothermic peak was 158.07 J g^{-1}. The degree of conversion of kaolinite dehydroxylation reaction and extracted aluminum increased as the calcination temperature and time increased, and the particles size was decreased. The optimum values of the degree of conversion of kaolinite dehydroxylation reaction and the extracted aluminum were 0.992 and 71.28% w/w, respectively, at the calcination conditions of 700°C, 180 min, and 106 μm. The degree of conversion of kaolinite dehydroxylation reaction and extracted aluminum results were well described by the response surface quadratic models. The results of optimum calcination conditions might be used to improve the subsequent aluminum extraction yield from calcined kaolinite with the hydrochloric acid dissolution method.

Acronyms

2FI: 2-Factor interactions
A: Absorbance
a, b, and c: Unit cell axes of the crystal system
Adj. R^2: Adjusted correlation coefficient
Al-ECR: Aluminum-eriochrome cyanine red complex
ANOVA: Analysis of variance
AP: Adequate precision
C: Concentration
Cor total SS: Sum of squares total corrected for the mean
CV: Coefficient of variance
Df: Degree of freedom
DSC: Differential scanning calorimetry
DTA: Differential thermogravimetry analyzer
Endo: Endothermic
Exo: Exothermic
FTIR: Fourier transformer infrared spectrometer
h_d: Enthalpy due to impurities removal from kaolinite
h_{de}: Enthalpy due to decomposition of aluminum chloride hexahydrate
h_p: Enthalpy due to dehydroxylation reaction of kaolinite
h_w: Enthalpy due to adsorbed water removal from kaolinite
LOI: Loss on ignition
m_f: Final mass of kaolinite sample after calcination
m_o: Initial mass of kaolinite sample
m_s: Residual mass loss of kaolinite sample
m_{smax}: Maximum mass loss of kaolinite sample
Pre.R^2: Predicted correlation coefficient
PRESS: Predicted residual sum of squares
R^2: Regression correlation coefficient
rpm: Revolution per minute
RSM-CCD: Response surface methodology with central composite design
SD: Standard deviation
S_j: Supplementary materials ($j = 1$–4)
TGA: Thermogravimetry analyzer
UV-vis: Ultraviolet-visible spectrophotometer
VIF: Variance inflation factor
% w/w: Percentage in mass basis
X_i: Coded form factors (temperature, time, and particles size)
XRD: X-ray diffractometer
XRF: X-ray fluorescence
Y: Dehydroxylation reaction degree of conversion
Z: Extracted aluminum
α, β, and γ: Unit cell angles of the crystal system
β_i: Linear coefficients in the model
β_{ij}: The quadratic coefficients in the model
β_j: Interactions' coefficients in the model
θ: Angle of peak position
λ: Wavelength of X-ray source.

Data Availability

The datasets generated during and/or analyzed during this study are available from the corresponding author upon request.

Conflicts of Interest

The authors declare that they have no conflicts of interest.

Acknowledgments

The authors like to thank Addis Ababa Science and Technology University to allow experimental set-up work and analytical instruments for characterization.

Supplementary Materials

Table S1. Summary of statistics in model selection for degree of conversion. Table S2. Quadratic model ANOVA analysis regression coefficient estimates, standard error, 95% CI, and VIF values for degree of conversion. Table S3. Summary of statistics analysis in model selection for extracted aluminum. Table S4. Quadratic model ANOVA analysis regression coefficient estimates, standard error, 95% CI, and VIF values for extracted aluminum. Figure S1. UV-vis spectra of maximum absorbance of (a) extracted aluminum and (b) standard aluminum chloride hexahydrate. Figure S2. Diagnostics plots for degree of conversion of (a) internally studentized residuals, (b) externally studentized residuals, (c) actual response values versus predicted response values, (d) predicted response values versus internally studentized residuals, (e) predicted response value versus externally studentized residuals, and (f) Box–Cox plot. Figure S3. Diagnostics plots for extracted aluminum: (a) internally studentized residuals, (b) externally studentized residuals, (c) actual response values versus predicted response values, (d) predicted response values versus internally studentized residuals, (e) predicted response values versus externally studentized residuals, and (f) Box–Cox plot. Figure S4.

Desirability plot for optimum values for both degree of conversion and extracted aluminum. (*Supplementary Materials*)

References

[1] K. Kyriakogona, I. Giannopoulou, and D. Panias, "Extraction of aluminium from kaolin: a comparative study of hydrometallurgical processes," in *Proceedings of the 3rd World Congress on Mechanical, Chemical, and Material Engineering*, vol. 17, pp. 8–10, Rome, Italy, June 2017.

[2] P. E. A. Lima, R. S. Angélica, and R. F. Neves, "Dissolution kinetics of Amazonian metakaolin in hydrochloric acid," *Clay Minerals*, vol. 52, no. 1, pp. 75–82, 2017.

[3] E. G. Pinna, D. S. Suarez, G. D. Rosales, and M. H. Rodriguez, "Hydrometallurgical extraction of Al and Si from kaolinitic clays," *REM-International Engineering Journal*, vol. 70, no. 4, pp. 451–457, 2017.

[4] M. C. Gastuche, F. Toussaint, J. Fripiat, R. Touilleaux, and M. Van Meersche, "Study of intermediate stages in the Kaolin⟶Metakaolin transformation," *Clay Minerals*, vol. 5, no. 29, pp. 227–236, 1963.

[5] Y. Cheng, J. Xing, C. Bu et al., "Dehydroxylation and structural distortion of kaolinite as a high-temperature sorbent in the furnace," *Minerals*, vol. 9, pp. 1–18, 2019.

[6] E. Gasparini, S. C. Tarantino, P. Ghigna et al., "Thermal dehydroxylation of kaolinite under isothermal conditions," *Applied Clay Science*, vol. 80-81, pp. 417–425, 2013.

[7] H. Rahier, B. Wullaert, and B. Van Mele, "Influence of the degree of dehydroxylation of kaolinite on the properties of aluminosilicate glasses," *Journal of Thermal Analysis and Calorimetry*, vol. 62, no. 2, pp. 417–427, 2000.

[8] S. A. Hosseini, A. Niaei, and D. Salari, "Production of γ-Al2O3 from kaolin," *Open Journal of Physical Chemistry*, vol. 01, no. 02, pp. 23–27, 2011.

[9] E. Santacesaria, D. Gelosa, and S. Carrà, "Basic behavior of alumina in the presence of strong acids," *Industrial and Engineering Chemistry Product Research and Development*, vol. 16, no. 1, pp. 45–47, 1977.

[10] J. Adeoye, J. Omoleye, and M. Ojewumi, "Development of alum from kaolin deposit using response surface methodology," *MOJ Bioorganic and Organic Chemistry*, vol. 2, pp. 167–170, 2018.

[11] R. O. Ajemba and O. D. Onukwuli, "Application of the shrinking core model to the analysis of alumina leaching from Ukpor clay using nitric acid," *International Journal of Engineering*, vol. 1, pp. 1–13, 2012a.

[12] A. Al-Zahrani and M. Abdelmajid, "Production of liquid alum coagulant from local Saudi clays," *Journal of King Abdulaziz University-Engineering Sciences*, vol. 15, no. 1, pp. 3–17, 2004.

[13] A. Mirwan, S. Susianto, A. Altway, and R. Handogo, "Kinetic model for identifying the rate controlling step of the aluminum leaching from peat clay," *Jurnal Teknologi*, vol. 80, pp. 37–44, 2018.

[14] P. E. A. Lima, R. S. Angélica, and R. F. Neves, "Dissolution kinetics of metakaolin in sulfuric acid: comparison between heterogeneous and homogeneous reaction methods," *Applied Clay Science*, vol. 88-89, pp. 159–162, 2014.

[15] P. E. A. Lima, R. S. Angélica, and R. F. Neves, "Dissolution kinetics of Amazonian metakaolin in nitric acid," *Cerâmica*, vol. 64, no. 369, pp. 86–90, 2018.

[16] V. I. Pak, S. S. Kirov, A. Y. Nalivaiko, D. Y. Ozherelkov, and A. A. Gromov, "Obtaining alumina from kaolin clay via aluminum chloride," *Materials*, vol. 12, pp. 1–12, 2019.

[17] S. A. Ajeel, F. A. Sameer, and N. I. AbdulLatif, "Separation of aluminum chloride from white kaolinite by slime leaching process," *Engineering and Technology Journal*, vol. 32, pp. 1707–1719, 2014.

[18] R. O. Ajemba and O. D. Onukwuli, "Kinetic model for Ukpor clay dissolution in hydrochlorlc acid solution," *Journal of Emerging Trends in Engineering and Applied Sciences*, vol. 3, pp. 448–454, 2012b.

[19] A. Ali, M. Al-Taie, and I. Ayoob, "The Extraction of alumina from kaolin," *Engineering and Technology Journal*, vol. 37, no. 4A, pp. 133–139, 2019.

[20] M. Lin, Y.-Y. Liu, S.-M. Lei, Z. Ye, Z.-Y. Pei, and B. Li, "High-efficiency extraction of Al from coal-series kaolinite and its kinetics by calcination and pressure acid leaching," *Applied Clay Science*, vol. 161, pp. 215–224, 2018.

[21] U. Mark, C. N. Anyakwo, O. O. Onyemaobi, and C. S. Nwobodo, "Effect of calcination condition on thermal activation of Ibere clay and dissolution of alumina," *International Journal of Nonferrous Metallurgy*, vol. 08, no. 02, pp. 9–24, 2019.

[22] M. Erdemoğlu, M. Birinci, and T. Uysal, "Thermal behavior of pyrophyllite ore during calcination for thermal activation for aluminum extraction by acid leaching," *Clays and Clay Minerals*, vol. 68, pp. 89–99, 2020.

[23] P. Si, X. Qiao, and J. Yu, "Alumina recovery from kaolin with mineral impurities," *Journal of Wuhan University of Technology*, vol. 27, no. 6, pp. 1139–1143, 2012.

[24] F. Chigondo, B. C. Nyamunda, and V. Bhebhe, "Extraction of water treatment coagulant from locally abundant kaolin clays," *Journal of Chemistry*, vol. 2015, Article ID 705837, 7 pages, 2015.

[25] A. Al-zahrani and M. Abdul-Majid, "Extraction of alumina from local clays by hydrochloric acid process," *Journal of King Abdulaziz University-Engineering Sciences*, vol. 20, no. 2, pp. 29–41, 2009.

[26] M. A. Tantawy and A. Ali Alomari, "Extraction of alumina from Nawan kaolin by acid leaching," *Oriental Journal of Chemistry*, vol. 35, no. 3, pp. 1013–1021, 2019.

[27] U. Udeigwe, O. Onukwuli, R. Ajemba, and C. Ude, "Kinetic studies of hydrochloric acid leaching of alumina from Agbaja clay," *International Journal of Research in Advanced Engineering and Technology*, vol. 1, pp. 64–72, 2015.

[28] T. A. Aragaw and A. A. Ayalew, "Removal of water hardness using zeolite synthesized from Ethiopian kaolin by hydrothermal method," *Water Practice and Technology*, vol. 14, no. 1, pp. 145–159, 2019.

[29] L. Ayele, J. Pérez-Pariente, Y. Chebude, and I. Díaz, "Synthesis of zeolite A from Ethiopian kaolin," *Microporous and Mesoporous Materials*, vol. 215, pp. 29–36, 2015.

[30] T. A. Aragaw and F. T. Angerasa, "Synthesis and characterization of Ethiopian kaolin for the removal of basic yellow (BY 28) dye from aqueous solution as a potential adsorbent," *Heliyon*, vol. 6, pp. 1–7, 2020.

[31] T. M. Zewdie, N. G. Habtu, A. Dutta, B. Van der Bruggen, and B. Van der Bruggen, "Characterization and beneficiation of Ethiopian kaolin for use in fabrication of ceramic membrane," *Materials Research Express*, vol. 11, no. 1, pp. 1–32, 2021.

[32] P. R. Bremner, L. J. Nicks, and D. J. Bauer, *A Basic Chloride Method for Extracting Aluminum from Clay*, Department of the Interior in Bureau of Mines Report of Investigtions (8866), USA, 1984.

[33] A. Ibrahim, I. Ibrahim, and A. Kandil, "Preparation of polyaluminum chlorides containing nano-Al_{13} from Egyptian kaolin and application in water treatment," *Technical Journal*

of Engineering and Applied Sciences, vol. 3, pp. 1194–1216, 2013.

[34] J. R. Mache, P. Signing, A. Njoya et al., "Smectite clay from the Sabga deposit (Cameroon): mineralogical and physico-chemical properties," *Clay Minerals*, vol. 48, no. 3, pp. 499–512, 2013.

[35] N. R. Osornio-Rubio, J. A. Torres-Ochoa, M. L. Palma-Tirado et al., "Study of the dehydroxylation of kaolinite and alunite from a Mexican clay with DRIFTS-MS," *Clay Minerals*, vol. 51, no. 1, pp. 55–68, 2016.

[36] W. Siriangkhawut, S. Tontrong, and P. Chantiratikul, "Quantitation of aluminium content in waters and soft drinks by spectrophotometry using eriochrome cyanine R," *Research Journal of Pharmaceutical, Biological and Chemical Sciences*, vol. 4, pp. 1155–1161, 2013.

[37] B. B. Kenne Diffo, A. Elimbi, M. Cyr, J. Dika Manga, and H. Tchakoute Kouamo, "Effect of the rate of calcination of kaolin on the properties of metakaolin-based geopolymers," *Journal of Asian Ceramic Societies*, vol. 3, no. 1, pp. 130–138, 2015.

[38] W. Chen, H. Zheng, J. Zhai et al., "Characterization and coagulation-flocculation performance of a composite coagulant: poly-ferric-aluminum-silicate-sulfate," *Desalination and Water Treatment*, vol. 56, no. 7, pp. 1776–1786, 2015.

[39] S. Yang, W. Li, H. Zhang, Y. Wen, and Y. Ni, "Treatment of paper mill wastewater using a composite inorganic coagulant prepared from steel mill waste pickling liquor," *Separation and Purification Technology*, vol. 209, pp. 238–245, 2019.

[40] M. Hartman, O. Trnka, and O. Šolcová, "Thermal decomposition of aluminum chloride hexahydrate," *Industrial & Engineering Chemistry Research*, vol. 44, no. 17, pp. 6591–6598, 2005.

[41] A. Tironi, M. A. Trezza, E. F. Irassar, and A. N. Scian, "Thermal treatment of kaolin: effect on the pozzolanic activity," *Procedia Materials Science*, vol. 1, pp. 343–350, 2012.

[42] H. Wang, C. Li, Z. Peng, and S. Zhang, "Characterization and thermal behavior of kaolin," *Journal of Thermal Analysis and Calorimetry*, vol. 105, no. 1, pp. 157–160, 2011.

[43] N. Zhang, Y. Yang, Z. Wang et al., "Study on the thermal decomposition of aluminium chloride hexahydrate," *Canadian Metallurgical Quarterly*, vol. 57, no. 2, pp. 235–244, 2018.

[44] S. T. Aly, I. A. Ibrahim, and M. F. Abadir, "Utilization of Kalapsha Kaolin to prepare high purity alumina," *Egyptian Journal of Chemistry*, vol. 62, pp. 1699–1712, 2019.

[45] K. M. Ibrahim, M. K. Moumani, and S. K. Mohammad, "Extraction of γ-Alumina from low–cost Kaolin," *Resources*, vol. 7, pp. 1–12, 2018.